Supplementary Material:

Interstitial vs. substitutional metal insertion in V_2O_5 as post-lithium ion battery cathode: a comparative GGA/GGA+U study with localized bases

Daniel Koch[a] and Sergei Manzhos [b]

a. Department of Mechanical Engineering, National University of Singapore, Block EA #07-08, 9 Engineering Drive 1, Singapore 117576. Email: koch.danielm@gmail.com

b. Centre Énergie Matériaux Télécommunications, Institut National de la Recherche Scientifique, 1650 boulevard Lionel-Boulet, Varennes QC J3X1S2 Canada. Email: sergei.manzhos@emt.inrs.ca

Computational setup

The computations in this work have been performed using density functional theory (DFT) with the exchange correlation functional of Perdew, Burke and Ernzerhof[1] (PBE) as implemented in the program package SIESTA 4.1[2] with Troullier-Martins pseudopotentials.[3] The basis set size was chosen as double-zeta and the real-space mesh cutoff set to 400 Ry. Insertion and substitution reactions were modelled in a 1x3x3 V_2O_5 supercell with a cell volume of ~12x11x14 $Å^3$ of the pristine compound while for the tuning of the Hubbard U parameter conventional unit cells of *Fm-3m* VO (8 atoms), *R-3c* V_2O_3 (30 atoms), *P4₂/mnm*VO_2 (12 atoms), and V_2O_5 (14 atoms) were employed. The k-point grids[4] in this work were generally found to sufficiently converge energy at ~30 points·Å per dimension. The pseudoatomic orbital (PAO) confinement energies[5-7] for the non-transition metals (Li, Na, Mg, Ca, and Al, as well as all the metal atoms in calculations for the empirical fitting of the molecular oxygen correction) were adjusted to match the experimentally observed cohesive energies of the respective bulk metals. The corresponding PAO energy shifts are 0.020 Ry for Li, 0.008 Ry for Na, 0.008 Ry for Mg, 0.030

Ry for Ca, 0.004 Ry for Al, 0.034 for Be, 0.060 for Ba, and 0.003 for Si. This approach to build the basis has been previously shown to reproduce experimental insertion energies and electronic structure well,[8-10] and it further ensures that the bulk metal reference energy, which is crucial for the determination of the dopant chemical potentials (see eq. (1)-(3) of the main text), is appropriately matched with experimental values. For V and O on the other hand, since either a Hubbard or an empirical correction, respectively, is applied to match experimental enthalpies, the PAO shift is set to 0.001 Ry corresponding to a relatively wide orbital confinement to minimize errors due to their finite support. The simplified rotationally invariant LDA+U approach proposed by Dudarev *et al*. was applied on V d states with pseudoatomic eigenstate projectors;[11] the magnitudes of U are reported at each instance. All structures have been subjected to ionic relaxation using a conjugate gradient algorithm with a force tolerance of 0.02 eV/Å and a stress threshold of 0.01 GPa. Partial occupancies were set with the Methfessel-Paxton method[12] and an electronic temperature of 500 K.

All-electron full-potential computations with a localized basis were performed for comparison using the PBE functional as implemented in the program package FHI-aims.[13, 14] A supercell with 16 formula units, a 3x3x3 k-point grid and light basis set definitions up to first tier for all species was used. Gaussian smearing was applied (broadening factor of 0.01), the atomic ZORA scalar relativistic treatment, and the geometry relaxed with a force tolerance of 0.02 eV/Å.[15-18]

Supporting hybrid functional computations were performed on the same 16 formula unit supercell using the Heyd-Scuseria-Erznerhof (HSE06) functional[19-21] as implemented in the program package VASP[22] using a plane wave basis set and the projector-augmented wave method.[23, 24] The structure was relaxed with a force tolerance of 0.05 eV/Å, a Gamma-only k point grid, and a plane wave cutoff energy of 500 eV. A Gaussian smearing with σ = 0.05 was

applied. Further computations with HSE06 were also performed using a localized basis in CRYSTAL17[25, 26] on a 3x3x3 k point mesh.[4] Truncation criteria for the Coulomb and exchange series of 10^{-7}, 10^{-7}, 10^{-7}, 10^{-7}, and 10^{-12} were applied[26] and a full geometry optimization with default convergence criteria (SCF and ionic) performed; an extra-extra-large grid generated with the atomic partition method by Becke[27-29] was used for real-space integration of the exchange-correlation contributions (99 radial points, 1454 angular points). The basis sets were chosen as Li_5-11(1d)G_baranek_2013_LiNbO3 (Li), O_8-411d1_bredow_2006 (O),[30] and V_86-411d4G_harrison_1993 (V),[31] denoted by the corresponding labels in the CRYSTAL online database (www.crystal.unito.it).

For the comparison with dispersion-corrected methods the ubiquitously used empirical D2 pair-potential method proposed by Grimme *et al.*,[32] as well as the *ab initio* van der Waals density functional vdW-DF-cx[33] (as implemented in SIESTA[34]) were used. The specific vdW-DF was chosen based on its reported ability to accurately reproduce the lattice parameters of layered compounds. Due to the problematic treatment of dispersion on (partially) ionized cations with predefined pair potentials,[35, 36] these were omitted and only interactions between the polarizable oxygen centers were subjected to the D2 correction. The interaction parameters for oxygen were adopted from Ref. [32].

Empirical correction for the GGA description of molecular oxygen

The DFT formation energies of the main group metal oxides Li_2O, Na_2O, BeO, MgO, CaO, BaO, Al_2O_3, and SiO_2 were calculated per O_2 molecule. The respective ground-state structures of the bulk metals and metal oxides were used as well as an isolated O_2 molecule. In Figure S1 the computed values are plotted against the respective experimental formation enthalpies reported in literature,[37-40] and the offset of the linear trendline (R^2 value of 0.89) from the main diagonal, found as 1.68 eV/molecule, was used as empirical correction for oxidation energies involving molecular oxygen in the subsequent calculations. The computed oxygen correction is larger in magnitude than what was previously reported in literature using a plane-wave setup and the projector-augmented wave method (-1.36 eV/molecule).[41]
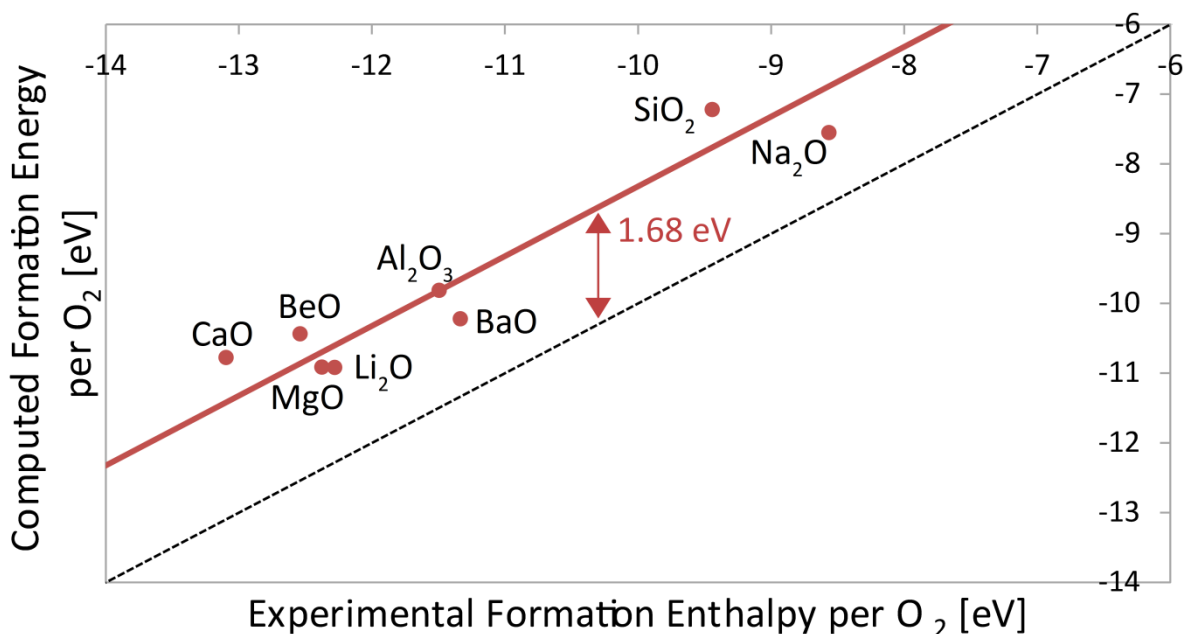
Figure S1. Computed formation energies of main group metal oxides (as indicated by labels) from bulk metal and O_2 plotted against their respective experimental values reported in literature. The trend line of the computed values is indicated as red, the main diagonal as black dashed line.

GGA vs. GGA+U results

In Table S computed properties of α-V_2O_5 with and without the adjusted Hubbard-U of 0.31 eV are compared to experimental values. The employed Hubbard correction has been found to have a negligible effect on the cell geometry and band gap. Additionally, low-concentration interstitial insertion voltages V for Li and Na in α-V_2O_5 against bulk metal (computed as insertion energy per transferred charge $V=-E_{ins}/q$) are compared to experimentally measured values (onset voltages of voltage-capacity curves) to give a further estimate of the accuracy of the computed thermochemistry data.

Table SI. Comparison of a, b, and c lattice parameters, band gap E_g, and onset cell voltage U of α-V_2O_5 against Li and Na bulk metal (high-concentration limit) computed with uncorrected and Hubbard-corrected PBE and experimental results for reference.

Property	PBE	PBE+U(=0.31 eV)	Experimental
a [Å]	11.679	11.676	11.512[42]
b [Å]	3.601	3.604	3.564[42]
c [Å]	4.614	4.614	4.368[42]
E_g [eV]	1.79	1.83	2.2-2.8[43, 44]
$V(Li_xV_2O_5)$ vs. Li^+/Li [V]	3.43	3.46	3.4[45]
$V(Na_xV_2O_5)$ vs. Na^+/Na [V]	3.47	3.51	3.6[46]

Generally, the small magnitude of the U parameter causes only minor deviations in all considered metrics. While the band gaps with and without Hubbard correction are both underestimated compared to the measured experimental reference, the lattice parameters and insertion energies are reproduced sufficiently well, suggesting that the uncorrected PBE results

5

with the chosen setup already provide a reliable estimate of reaction energetics. In Figure S2(b) the densities of states (DOS) computed with PBE and PBE+U are compared for the lithiated V_2O_5 supercell. The Hubbard correction causes a slight shift of the occupied state deeper into the band gap, while for the uncorrected DOS localized state and conduction band minimum are in close proximity. The spin density for this system in Figure S2(a) obtained with the uncorrected PBE functional shows a localized electron state distributed over a V-O-V fragment in the V_2O_5 structure. This type of localization pattern has been previously described in theoretical literature using the established approach of Hubbard-corrected GGA functionals (with plane-waves) for monovalent metal insertion in α-V_2O_5[47, 48] and is reminiscent of the experimentally observed charge ordering in α'-NaV_2O_5 at T > 34 K.[49-52] The Mulliken charges of the vanadium centers indicate a magnetic moment of ~0.8 μ_B for each of the cations on the spin-polarized V-O-V rung, while the bridging and axial oxygen centers of the fragment carry in total ~-0.6 μ_B, resulting in a total magnetic moment of 1.0 μ_B as the magnetic moments of all other ions are found to be negligible.
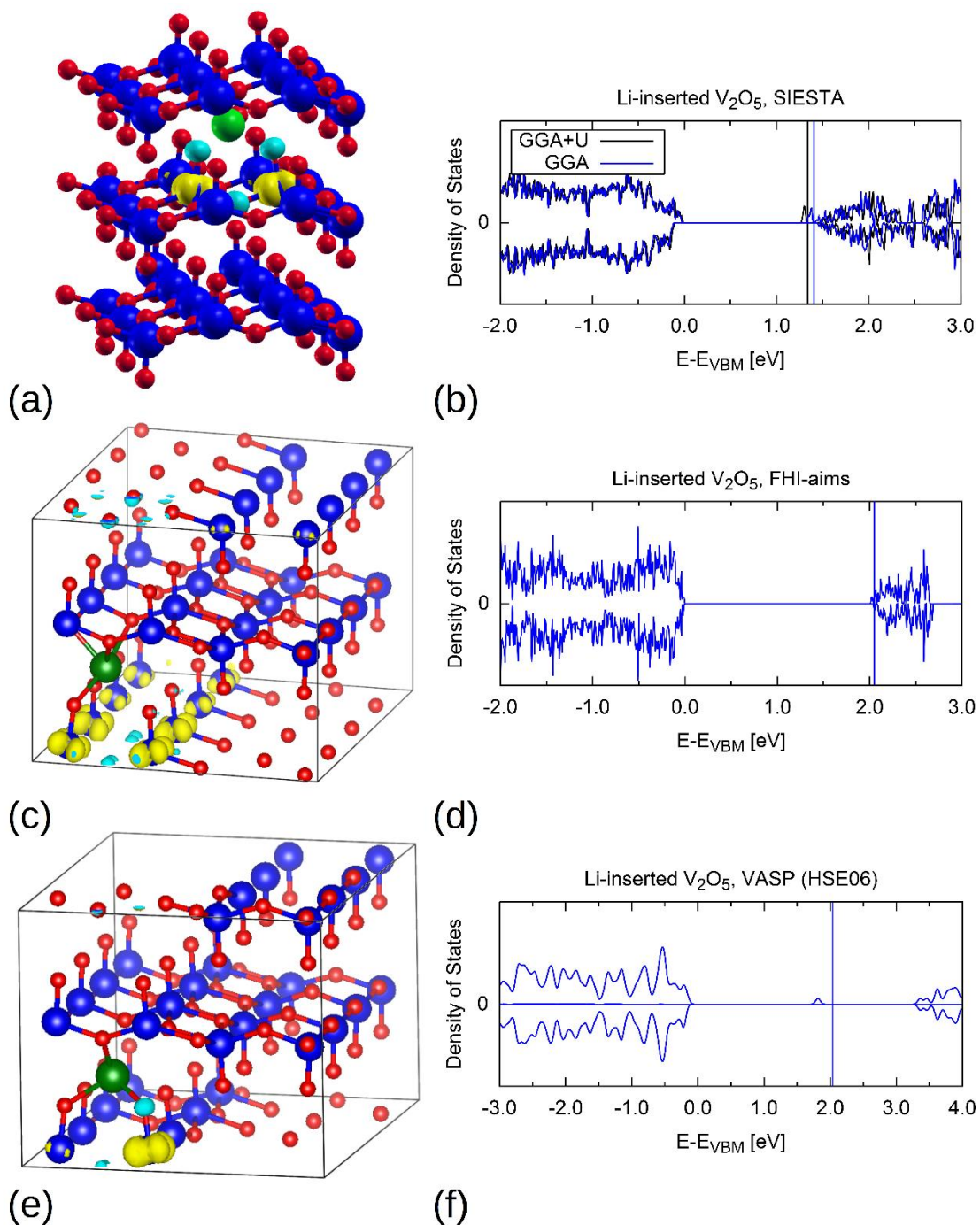
Figure S2. (a) GGA-computed isosurface plot of the spin density of Li-inserted V_2O_5 (isovalue: 0.01 e/Å^{-3}), and (b) density of states obtained with the PBE density functional with (black) and without (blue) applied Hubbard U as obtained in the program package SIESTA. (c) Spin density and (d) density of states of a lithiated V_2O_5 supercell computed with pure PBE in the all-electron program package FHI-aims; (e) spin density and (f) density of states computed with the HSE06 hybrid functional in the program package VASP using a plane wave basis and the projector-augmented wave method.

Comparison with the all-electron full-potential results in Figure S2(c) and (d) (see computational details above) shows a rather localized state as well, with most of the charge spread over the vanadium centers close to the intercalated Li, but the localization pattern is less sharp than computed in SIESTA. Furthermore, there is a less clear separation of the occupied state from the conduction band minimum in Figure S2(d), suggesting a somewhat less localized electron in the all-electron full-potential case. Besides differences in electronic structure, the position of the Li intercalant is shifted from the center of the insertion site towards a fourfold coordinated position with PBE in FHI-aims which is frequently reported for the Li insertion in V_2O_5 modelled with GGA+U, although in these computations the asymmetric coordination is related to the position of an electron-polaron localized on one distinct V center.[53, 54] The latter does not apply here, and the reason for the computed off-center shift of the Li ion remains unclear, possibly requiring further investigations which are beyond the scope of this work. However, the comparison suggests that on one hand localized bases predict certain aspects of atomistic or electronic structure on metalated V_2O_5 in agreement with Hubbard-corrected plane-wave PBE, but on the other hand code-dependent computational specifics cause certain differences between the computation results. Therefore, particulars of the SIESTA program package like the used pseudopotentials or basis set definitions might contribute to the observed agreement of the PBE results with experimental and GGA+U results in literature.

Computations using the HSE06 hybrid functional with plane-wave as well as localized basis functions as implemented in the program packages VASP and CRYSTAL17, respectively, show on the other hand a localization of the donated electron on a single vanadium center. Mulliken charges indicate a magnetization of ~1 μ_B of one vanadium center next to the Li intercalant in both cases. The spin density obtained with plane waves and the projector augmented wave method is shown in Figure S2(e). Details of the hybrid functional calculations

are provided in the computational setup section above. The computed hybrid functional band gap shown in Figure S2(f) is larger than with the GGA+U setup used in this work and, as expected, in better agreement with experimental results (see Table SI), resulting in a larger energy difference between localized mid-gap state and conduction band minimum. The single-cation reduction in lithiated V_2O_5 has been reported in theoretical literature with Hubbard-corrected GGA before,[53, 54] but experimental data actually suggests the delocalization of one electron over four neighboring vanadium centers in $M_xV_2O_5$ at low concentrations of inserted monovalent cations M ($x \sim 0.01$) like Li^+ or Cu^+.[55-58] The commonly reported confinement to a single vanadium center hence would be an artificial overlocalization obtained with Hubbard-corrected GGA and hybrid functionals. The two-center delocalization in SIESTA, while not in exact agreement with experimental findings, reflects the electron donation to multiple vanadium centers in the low-concentration limit at least in part. Furthermore, the slightly higher dopant concentration in our simulation cell than in experimental literature and the higher temperatures at which these experiments in Refs. [55-58] were conducted still do not rule out a possible partial delocalization of one electron over a V-O-V fragment in our $Li_{0.06}V_2O_5$ cell at 0 K. In any case, it does not make our results less reliable compared to commonly used approaches like plane-wave GGA+U with large magnitudes of U or even hybrid calculations.

Effect of dispersion corrections

In Table SII the computed lattice parameters of pristine and lithiated vanadium pentoxide are compared with and without dispersion corrections. The additional dispersive interactions were modelled by an empirical pair potential (D2) in combination with PBE and a van der Waals density functional (vdw-DF-cx). A Hubbard correction with the previously tuned parameter U=0.31 eV on vanadium d states was applied in all computations. For details on the employed methods see the supplementary computational setup section above. As can be seen, the computed insertion energies are in close agreement with each other and also with the experimentally reported value. This is an important condition since this work is mainly concerned with the energetics of V_2O_5 doping. However, the additional dispersion interactions either have a negligible effect on geometries, which is the case for PBE-D2 with standard parameters for oxygen-oxygen interactions, or significantly underestimate the c lattice parameter due to exaggerated interlayer binding, as it can be seen with vdW-DF-cx. Although the magnitude of the deviation in c direction is slightly smaller with vdW-DF-cx (~4%) than with PBE (~6%), a clear improvement could not be obtained while on the other hand the computational cost is raised with the vdW-DF compared to PBE.[34] In addition, experimental lattice parameters for a low-concentration $Li_{0.17}V_2O_5$ phase obtained by electroreduction are included in Table SII as reference for the dilute-limit geometries.[59] While the Li content of the experimental phase is higher than in the simulation cell ($Li_{0.06}V_2O_5$), it nevertheless allows for a qualitative comparison of the correct geometry change behavior with increasing Li content. The changes computed with the chosen methods are all in the same regime and correctly reproduce an expansion in c direction while failing to predict the expansion in a and contraction in b direction in the dilute limit. All in all, the tested dispersion-corrected methods do not provide cell geometries or their

qualitative changes, while correctly reproducing insertion energies, significantly more accurately

than dispersion-uncorrected PBE.

Table SII. Comparison of *a*, *b*, and *c* lattice parameters in pristine and lithiated V_2O_5, as well as low-concentration Li insertion energies, computed with PBE, empirically dispersion-corrected PBE-D2, the van der Waals-functional vdW-DF-cx, and experimentally observed values reported in literature. The previously tuned Hubbard correction with U=3.10 eV was applied in all computations. The low-concentration stoichiometric coefficient for Li in the computed supercell is x=0.06, for the experimental reference value x=0.17.

System	Property	PBE+U	PBE-D2+U	vdW-DF-cx+U	Experimental
V_2O_5	a [Å]	11.676	11.678	11.764	11.512[42]
	b [Å]	3.604	3.604	3.597	3.564[42]
	c [Å]	4.614	4.600	4.220	4.368[42]
$Li_xV_2O_5$	a [Å]	11.648	11.651	11.720	11.520[59]
	b [Å]	3.606	3.606	3.600	3.554[59]
	c [Å]	4.643	4.624	4.253	4.380[59]
	E_{Li}^{ins}[eV/atom]	-3.43	-3.46	-3.40	-3.4[45]

Comparison of computed insertion energies to existing literature

In Table SI the insertion energies computed in this work are compared to the range of theoretical values found in existing literature. The values computed in this work are in good agreement with the values found in previous reports which were all obtained from plane-wave GGA setups of different flavors. The only exception is the dilute-limit Al insertion energy, which was found smaller than in a previous study. However, the Al insertion energy value computed in this work is in better agreement with the experimentally observed voltages (which are sensitive indicators of insertion energies), commonly reported lower in the low-concentration regime than what the previously computed value suggests,[60, 61] while again other theoretical studies have not even found any thermodynamically favorable insertion of Al in α-V_2O_5,[62, 63] which is not supported by experimental findings as well.

Table SIII. Comparison between insertion energies for the studied Li, Na, Mg, Ca, and Al dopants in α-V_2O_5 with a bulk metal reference state computed in the present work and in previous theoretical studies. The methods used to obtain the theoretical reference energies are indicated in parentheses behind the corresponding values.

Low-concentration phase	Insertion energies in this work [eV/atom]	Insertion energies in previous studies [eV/atom]
$Li_xV_2O_5$	-3.46	-3.24 (PBE+U),[64]
		-3.50 (optPBE-vdW+U),[64]
		-3.13 (PBEsol+U),[65]
		-3.43 (PBE),[66]
		-3.23 (PBE-D3)[67]
$Na_xV_2O_5$	-3.50	-3.32 (PBE+U),[64]
		-3.62 (optPBE-vdW+U),[64]
		-3.17 (PBEsol+U),[65]

		-2.85 (PBE-vdW+U)[68]
		-3.39 (PBE-D3)[67]
$Mg_xV_2O_5$	-5.02	-4.99 (PBE+U),[64]
		-4.54 (PBE+U, MgV_2O_5),[69]
		-5.39 (optPBE-vdW+U),[64]
		-5.50 (PBEsol+U),[65]
		-4.50 (PBE),[66]
		-4.68 (PBE-D3)[67]
$Ca_xV_2O_5$	-6.84	-4.92 (PBE+U),[64]
		-5.57 (optPBE-vdW+U),[64]
		-6.53 (PBE-vdW+U)[68]
		-6.14 (PBE+U-D2)[70]
$Al_xV_2O_5$	-3.83	-5.11 (PBEsol+U)[65]

References

1.   J.P. Perdew, K. Burke and M. Ernzerhof: Generalized Gradient Approximation Made Simple. *Phys. Rev. Lett.* **77**, 3865 (1996).

2.   J.M. Soler, E. Artacho, J.D. Gale, A. García, J. Junquera, P. Ordejón and D. Sánchez-Portal: The SIESTA method for ab initio order-N materials simulation. *J. Phys.: Condens. Matter* **14**, 2745 (2002).

3.   N. Troullier and J.L. Martins: Efficient pseudopotentials for plane-wave calculations. *Phys. Rev. B* **43**, 1993 (1991).

4.   H.J. Monkhorst and J.D. Pack: Special points for Brillouin-zone integrations. *Phys. Rev. B* **13**, 5188 (1976).

5.   E. Anglada, J. M. Soler, J. Junquera and E. Artacho: Systematic generation of finite-range atomic basis sets for linear-scaling calculations. *Phys. Rev. B* **66**, 205101 (2002).

6.   E. Artacho, D. Sánchez-Portal, P. Ordejón, A. García and J.M. Soler: Linear-Scaling ab-initio Calculations for Large and Complex Systems. *Phys. Status Solidi B* **215**, 809 (1999).

7.   J. Junquera, Ó. Paz, D. Sánchez-Portal and E. Artacho: Numerical atomic orbitals for linear-scaling calculations. *Phys. Rev. B* **64**, 235111 (2001).

8.   D. Koch and S. Manzhos: Can Doping of Transition Metal Oxide Cathode Materials Increase Achievable Voltages with Multivalent Metals? *ChemRxiv.* **Preprint.** (2019). doi:10.26434/chemrxiv.10050575.v1.

9.   D. Koch and S. Manzhos: A Comparative First-Principles Study of Lithium, Sodium and Magnesium Insertion Energetics in Brookite Titanium Dioxide. *MRS Adv.* **4**, 837 (2019).

10.   F. Legrain and S. Manzhos: A first-principles comparative study of lithium, sodium, and magnesium storage in pure and gallium-doped germanium: Competition between interstitial and substitutional sites. *J. Chem. Phys.* **146**, 034706 (2017).

11.   S.L. Dudarev, G.A. Botton, S.Y. Savrasov, C.J. Humphreys and A.P. Sutton: Electron-energy-loss spectra and the structural stability of nickel oxide: An LSDA+U study. *Phys. Rev. B* **57**, 1505 (1998).

12.   M. Methfessel and A.T. Paxton: High-precision sampling for Brillouin-zone integration in metals. *Phys. Rev. B* **40**, 3616 (1989).

13. V. Blum, R. Gehrke, F. Hanke, P. Havu, V. Havu, X. Ren, K. Reuter and M. Scheffler: Ab initio molecular simulations with numeric atom-centered orbitals. *Comput. Phys. Commun.* **180**, 2175 (2009).

14. V. Havu, V. Blum, P. Havu and M. Scheffler: Efficient O(N) integration for all-electron electronic structure calculation using numeric basis functions. *J. Comput. Phys.* **228**, 8367 (2009).

15. C. Chang, M. Pelissier and P. Durand: Regular Two-Component Pauli-Like Effective Hamiltonians in Dirac Theory. *Phys. Scr.* **34**, 394 (1986).

16. J.L. Heully, I. Lindgren, E. Lindroth, S. Lundqvist and A.M. Martensson-Pendrill: Diagonalisation of the Dirac Hamiltonian as a basis for a relativistic many-body procedure. *J. Phys. B: Atom. Mol. Phys.* **19**, 2799 (1986).

17. E. van Lenthe, E.J. Baerends and J.G. Snijders: Relativistic total energy using regular approximations. *J. Chem. Phys.* **101**, 9783 (1994).

18. E. van Lenthe, J.G. Snijders and E.J. Baerends: The zero-order regular approximation for relativistic effects: The effect of spin–orbit coupling in closed shell molecules. *J. Chem. Phys.* **105**, 6505 (1996).

19. J. Heyd, G.E. Scuseria and M. Ernzerhof: Hybrid functionals based on a screened Coulomb potential. *J. Chem. Phys.* **118**, 8207 (2003).

20. J. Heyd, G.E. Scuseria and M. Ernzerhof: Erratum: "Hybrid functionals based on a screened Coulomb potential" [J. Chem. Phys. 118, 8207 (2003)]. *J. Chem. Phys.* **124**, 219906 (2006).

21. J. Paier, M. Marsman, K. Hummer, G. Kresse, I.C. Gerber and J.G. Ángyán: Screened hybrid density functionals applied to solids. *J. Chem. Phys.* **124**, 154709 (2006).

22. G. Kresse and J. Furthmüller: Efficient iterative schemes for ab initio total-energy calculations using a plane-wave basis set. *Phys. Rev. B* **54**, 11169 (1996).

23. P.E. Blöchl: Projector augmented-wave method. *Phys. Rev. B* **50**, 17953 (1994).

24. G. Kresse and D. Joubert: From ultrasoft pseudopotentials to the projector augmented-wave method. *Phys. Rev. B* **59**, 1758 (1999).

25. R. Dovesi, A. Erba, R. Orlando, C.M. Zicovich-Wilson, B. Civalleri, L. Maschio, M. Rérat, S. Casassa, J. Baima, S. Salustro and B. Kirtman: Quantum-mechanical condensed matter simulations with CRYSTAL. *WIREs Computational Molecular Science* **8**, e1360 (2018).

26. R. Dovesi, V.R. Saunders, C. Roetti, R. Orlando, C.M. Zicovich-Wilson, F. Pascale, B. Civalleri, K. Doll, N.M. Harrison, I.J. Bush, P. D'Arco, M. Llunell, M. Causà, Y. Noël, L. Maschio, A. Erba, M. Rerat and S. Casassa: CRYSTAL17 User's Manual, (University of Torino, Torino, 2017).

27. A.D. Becke: A multicenter numerical integration scheme for polyatomic molecules. *J. Chem. Phys.* **88**, 2547 (1988).

28. A.D. Becke: Correlation energy of an inhomogeneous electron gas: A coordinate-space model. *J. Chem. Phys.* **88**, 1053 (1988).

29. M.D. Towler, A. Zupan and M. Causà: Density functional theory in periodic systems using local Gaussian basis sets. *Comput. Phys. Commun.* **98**, 181 (1996).

30. T. Bredow, K. Jug and R.A. Evarestov: Electronic and magnetic structure of ScMnO3. *Phys. Status Solidi B* **243**, R10 (2006).

31. W.C. Mackrodt, N.M. Harrison, V.R. Saunders, N.L. Allan, M.D. Towler, E. Aprà and R. Dovesi: Ab initio Hartree-Fock calculations of CaO, VO, MnO and NiO. *Philos. Mag. A* **68**, 653 (1993).

32. S. Grimme: Semiempirical GGA-type density functional constructed with a long-range dispersion correction. *J. Comput. Chem.* **27**, 1787 (2006).

33. K. Berland and P. Hyldgaard: Exchange functional that tests the robustness of the plasmon description of the van der Waals density functional. *Phys. Rev. B* **89**, 035412 (2014).

34. G. Román-Pérez and J.M. Soler: Efficient Implementation of a van der Waals Density Functional: Application to Double-Wall Carbon Nanotubes. *Phys. Rev. Lett.* **103**, 096102 (2009).

35. S. Ehrlich, J. Moellmann, W. Reckien, T. Bredow and S. Grimme: System-Dependent Dispersion Coefficients for the DFT-D3 Treatment of Adsorption Processes on Ionic Surfaces. *ChemPhysChem* **12**, 3414 (2011).

36. S. Grimme, J. Antony, S. Ehrlich and H. Krieg: A consistent and accurate ab initio parametrization of density functional dispersion correction (DFT-D) for the 94 elements H-Pu. *J. Chem. Phys.* **132**, 154104 (2010).

37. G.K. Johnson, R.T. Grow and W.N. Hubbard: The enthalpy of formation of lithium oxide (Li_2O). *J. Chem. Thermodyn.* **7**, 781 (1975).

38. P.A.G. O'Hare: Thermochemical and Theoretical Investigations of the Sodium-Oxygen System. I. The Standard Enthalpy of Formation of Sodium Oxide (Na_2O). *J. Chem. Phys.* **56**, 4513 (1972).

39. R.C. Ropp: Chapter 3 - Group 16 (O, S, Se, Te) Alkaline Earth Compounds, in Encyclopedia of the Alkaline Earth Compounds, edited by R. C. Ropp (Elsevier, Amsterdam, 2013), pp. 105.

40. M.W. Chase Jr.: NIST-JANAF thermochemical tables, 4th ed. (Washington, DC: American Chemical Society; New York: American Institute of Physics for the National Institute of Standards and Technology, 1998).

41. L. Wang, T. Maxisch and G. Ceder: Oxidation energies of transition metal oxides within the GGA+U framework. *Phys. Rev. B* **73**, 195107 (2006).

42. R. Enjalbert and J. Galy: A refinement of the structure of V_2O_5. *Acta Crystallogr. C* **42**, 1467 (1986).

43. E.E. Chain: Optical properties of vanadium dioxide and vanadium pentoxide thin films. *Appl. Opt.* **30**, 2782 (1991).

44. J. Meyer, K. Zilberberg, T. Riedl and A. Kahn: Electronic structure of Vanadium pentoxide: An efficient hole injector for organic electronic materials. *J. Appl. Phys.* **110**, 033710 (2011).

45. C. Delmas, H. Cognac-Auradou, J.M. Cocciantelli, M. Ménétrier and J.P. Doumerc: The $Li_xV_2O_5$ system: An overview of the structure modifications induced by the lithium intercalation. *Solid State Ion.* **69**, 257 (1994).

46. S. Liu, Z. Tong, J. Zhao, X. Liu, J. wang, X. Ma, C. Chi, Y. Yang, X. Liu and Y. Li: Rational selection of amorphous or crystalline V_2O_5 cathode for sodium-ion batteries. *Phys. Chem. Chem. Phys.* **18**, 25645 (2016).

47. X. Ming, H.-G. Fan, Z.-F. Huang, F. Hu, C.-Z. Wang and G. Chen: Magnetic gap in Slater insulator α′-NaV_2O_5. *J. Phys.: Condens. Matter* **20**, 155203 (2008).

48. D. Koch, V.V. Kulish and S. Manzhos: A first-principles study of potassium insertion in crystalline vanadium oxide phases as possible potassium-ion battery cathode materials. *MRS Commun.* **7**, 819 (2017).

49. J.L. de Boer, A. Meetsma, J. Baas and T.T.M. Palstra: Spin-Singlet Clusters in the Ladder Compound NaV_2O_5. *Phys. Rev. Lett.* **84**, 3962 (2000).

50. M. Lohmann, H.A. Krug von Nidda, M.V. Eremin, A. Loidl, G. Obermeier and S. Horn: Charge Order in NaV_2O_5 Studied by EPR. *Phys. Rev. Lett.* **85**, 1742 (2000).

51. H. Nakao, K. Ohwada, N. Takesue, Y. Fujii, M. Isobe, Y. Ueda, M.v. Zimmermann, J.P. Hill, D. Gibbs, J.C. Woicik, I. Koyama and Y. Murakami: X-Ray Anomalous Scattering Study of a Charge-Ordered State in NaV_2O_5. *Phys. Rev. Lett.* **85**, 4349 (2000).

52. T. Ohama, H. Yasuoka, M. Isobe and Y. Ueda: Mixed valency and charge ordering in α-NaV_2O_5. *Phys. Rev. B* **59**, 3299 (1999).

53. D.O. Scanlon, A. Walsh, B.J. Morgan and G.W. Watson: An ab initio Study of Reduction of V_2O_5 through the Formation of Oxygen Vacancies and Li Intercalation. *J. Phys. Chem. C* **112**, 9903 (2008).

54. S. Suthirakun, A. Genest and N. Rösch: Modeling Polaron-Coupled Li Cation Diffusion in V_2O_5 Cathode Material. *J. Phys. Chem. C* **122**, 150 (2018).

55. D. Gourier, A. Tranchant, N. Baffier and R. Messina: EPR study of electrochemical lithium intercalation in V_2O_5 cathodes. *Electrochim. Acta* **37**, 2755 (1992).

56. V.S. Grunin, I.B. Patrina and Z.N. Zonn: Impurities and electron localization in V_2O_5 crystals. *Phys. Status Solidi B* **115**, 545 (1983).

57. J.L. Ragle: Electron Spin Resonance Study of Partially Reduced Vanadium Pentoxide. *J. Chem. Phys.* **38**, 2020 (1963).

58. G. Sperlich and W.D. Lazé: Estimate of the d–d Overlap of V_2O_5 from ESR Measurements. *Phys. Status Solidi B* **65**, 625 (1974).

59. S. Hub, A. Tranchant and R. Messina: X-ray investigations on electroformed $Li_xV_2O_5$ bronzes. *Electrochim. Acta* **33**, 997 (1988).

60. S. Gu, H. Wang, C. Wu, Y. Bai, H. Li and F. Wu: Confirming reversible Al^{3+} storage mechanism through intercalation of Al^{3+} into V_2O_5 nanowires in a rechargeable aluminum battery. *Energy Storage Materials* **6**, 9 (2017).

61. H. Wang, Y. Bai, S. Chen, X. Luo, C. Wu, F. Wu, J. Lu and K. Amine: Binder-Free V_2O_5 Cathode for Greener Rechargeable Aluminum Battery. *ACS Appl. Mater. Interface* **7**, 80 (2015).

62. G.S. Gautam, P. Canepa, R. Malik, M. Liu, K. Persson and G. Ceder: First-principles evaluation of multi-valent cation insertion into orthorhombic V_2O_5. *Chem. Commun.* **51**, 13619 (2015).

63. Z. Rong, R. Malik, P. Canepa, G. Sai Gautam, M. Liu, A. Jain, K. Persson and G. Ceder: Materials Design Rules for Multivalent Ion Mobility in Intercalation Structures. *Chem. Mater.* **27**, 6016 (2015).

64. J. Carrasco: Role of van der Waals Forces in Thermodynamics and Kinetics of Layered Transition Metal Oxide Electrodes: Alkali and Alkaline-Earth Ion Insertion into V_2O_5. *J. Phys. Chem. C* **118**, 19599 (2014).

65. Vadym V. Kulish and S. Manzhos: Comparison of Li, Na, Mg and Al-ion insertion in vanadium pentoxides and vanadium dioxides. *RSC Adv.* **7**, 18643 (2017).

66. R. Xiao, J. Xie, T. Luo, L. Huang, Y. Zhou, D. Yu, C. Chen and Y. Liu: Phase Transformation and Diffusion Kinetics of V_2O_5 Electrode in Rechargeable Li and Mg Batteries: A First-Principle Study. *J. Phys. Chem. C* **122**, 1513 (2018).

67. X. Zhao, X. Zhang, D. Wu, H. Zhang, F. Ding and Z. Zhou: Ab initio investigations on bulk and monolayer V_2O_5 as cathode materials for Li-, Na-, K- and Mg-ion batteries. *J. Mater. Chem. A* **4**, 16606 (2016).

68. D. Wang, H. Liu, J.D. Elliott, L.-M. Liu and W.-M. Lau: Robust vanadium pentoxide electrodes for sodium and calcium ion batteries: thermodynamic and diffusion mechanical insights. *J. Mater. Chem. A* **4**, 12516 (2016).

69. G. Sai Gautam, P. Canepa, A. Abdellahi, A. Urban, R. Malik and G. Ceder: The Intercalation Phase Diagram of Mg in V_2O_5 from First-Principles. *Chem. Mater.* **27**, 3733 (2015).

70. D. Koch and S. Manzhos: First-Principles Study of the Calcium Insertion in Layered and Non-Layered Phases of Vanadia. *MRS Adv.* **3**, 3507 (2018).